Letter

Velocimetry using free-induction decay of matter-wave lattices

Gehrig Carlse,* Jaskaran Randhawa, Eduardo Ramos, Thomas Vacheresse, Alex Pouliot, and A. Kumarakrishnan†
Department of Physics and Astronomy, York University, Toronto, Ontario, Canada M3J 1P3

(Received 25 November 2024; accepted 10 February 2025; published 24 February 2025)

We demonstrate a matter-wave velocimeter which probes the free-induction decay of an atomic lattice formed by interaction with an optical standing wave in the reference frame of the laser-cooled sample. During the drop time of the atoms in a gravitational field, we ensure lattice formation by changing the relative detuning of counterpropagating components of the standing wave. The contrast of the lattice, which is sensitive to the first-order Doppler shift, is measured by backscattering a near-resonant traveling-wave electric field. We infer the center-of-mass velocity by determining the line center of the backscattered spectrum. By varying the drop time, we also measure the gravitational acceleration of the falling lattice. We find that the spectrum can be considerably narrowed by imprinting a Ramsey fringe using two time-separated excitation pulses. We demonstrate these ideas using a sample of rubidium atoms with a temperature of ∼10 μK, achieving a precision of 600 μm/s for measurements of velocity and 2 mm/s^2 for determinations of gravity. Since the primary limitation in precision relates to the thermal coherence length of the sample, we show that the most precise atomic velocimeter can be realized by applying these techniques to a typical Bose gas.

DOI: 10.1103/PhysRevA.111.L021304

The transition to quantum metrology is well underway and atoms have become the basis for a new generation of motional and intertial sensors. The realization of atom interferometers to measure gravitational acceleration (g) [1–3], gravity gradients [4,5], and rotations [6–8], including multiaxis inertial sensing [9,10], has paved the way for compact and portable sensors [11–16]. In addition, large-scale interferometers that are designed to allow atoms to fall through long drop distances [17–19], have also been developed to test fundamental interactions [20–25]. These breath-taking experiments implicitly rely upon the phase stability of an inertial reference frame which must be maintained over the timescale of the experiment [26]. To overcome this challenge, accelerometers that are based on velocimetry have gained interest due to their potential insensitivity to mechanical vibrations and the possibility of avoiding phase monitoring and postcorrection [27,28].

Such velocimeters derive their precision either by monitoring the optical phase of a probe beam interacting with a moving sample such as in the investigations of electromagnetically induced transparency [29,30] or from the observation of the Doppler shift of a narrow transition between two ground states as in velocity selection experiments in Ref. [31]. This latter technique is an integral step in Raman atom interferometery [1] and precise frequency domain velocimetry [32,33]. Separately, a class of time domain atom interferometer experiments have also realized measurements of velocity by observing the linearly incrementing phase of light scattered from a falling atomic lattice [34,35].

In this Letter, we describe particularly simple ideas for velocimetry which rely on measuring the contrast of an atomic lattice, formed due to matter-wave interference between momentum states following a standing-wave excitation of the sample [36,37]. The contrast of such a lattice can be probed by backscattering a traveling-wave readout pulse and measuring the free-induction decay (FID) from the phased array of radiating atoms. The decay of the lattice is therefore governed by the time it takes a typical atom to move one period of the lattice spacing. While the transient nature of this lattice has been exploited in echo experiments [35,36,38–43], we find that the time constant of the FID is sufficiently long for imprinting and extracting specific variations in the lattice contrast.

By creating the standing wave using counterpropagating laser pulses with identical frequencies in the reference frame of the atomic sample, the lattice forms in a single hyperfine ground state, as shown in Fig. 1(a). The velocity sensitivity of the lattice contrast arises from the differential detuning of counterpropagating laser pulses experienced by a moving atomic sample. As the sample falls, the two-photon resonance can be maintained by changing the relative detuning of counterpropagating components of the standing wave.

For excitation laser pulses detuned far from excited-state resonances of the sample, the contrast of the ensuing lattice can be expressed as

$$\mathcal{C}(\tau, \Delta_0) \propto \left(\frac{\sin \Delta_0 \tau}{\Delta_0 \tau}\right)^2, \tag{1}$$

where τ is the excitation pulse width, $\Delta_0 = \nu_2(1 + v/c) - \nu_1(1 - v/c)$ is the difference in frequency between the counterpropagating laser pulses in the frame of reference of the sample, and c is the speed of light. This is the well-known spectral response of a two-level atom exposed to a laser field, which, in this work, is imprinted on the lattice formed in the atomic ground state.

*Contact author: gehrig.carlse@gmail.com
†Contact author: akumar@yorku.ca

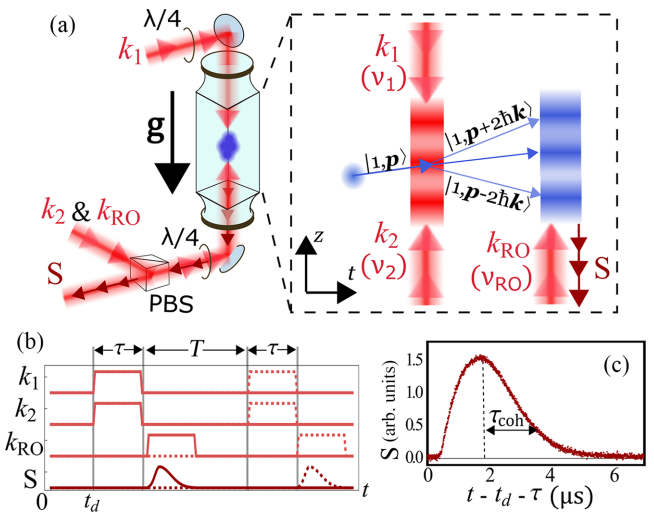

FIG. 1. (a) Schematic of the experimental setup for the matter-wave velocimeter. The excitation beams (k_1 and k_2) and readout beam (k_{RO}), shown by transparent red arrows, are aligned along the vertical (z) direction. The backscattered field (S) is shown by solid maroon arrows reflecting from the atomic lattice (purple). PBS: polarizing beam splitter. $\lambda/4$: quarter-wave plate. Inset: Lattice formation arising from matter-wave interference of a single ground state $|1, \boldsymbol{p}\rangle$. Counterpropagating components of the excitation have frequencies ν_1 and ν_2 in the laboratory frame, both far detuned from the ground-excited-state resonance. (b) Optical pulse sequence for the single-pulse (solid lines) and TSOF (dashed lines) configurations of the velocimeter at a drop time t_d, where the cold sample is released at $t = 0$. (c) Time evolution of the backscattered signal in the single-pulse velocimeter, showing the FID of the lattice with time constant τ_{coh}.

The lattice contrast can then be inferred by measuring the intensity of backscattered light from a traveling-wave readout pulse, as shown in Fig. 1.

In this case, the center-of-mass (c.m.) velocity of the sample can be extracted from the expression for the central maximum of the contrast spectrum

$$v = \left(\frac{-\Delta}{\nu_2 + \nu_1}\right)c, \tag{2}$$

where $\Delta = \nu_2 - \nu_1$ is the relative frequency difference in the laboratory frame and $\Delta_0 = \Delta + \frac{v}{c}(\nu_1 + \nu_2)$.

Therefore a single-pulse c.m. velocimeter can be realized on the basis of Eqs. (1) and (2), by determining the line center of the lattice contrast as a function of the laboratory-frame detuning. By measuring the velocity as a function of the time spent falling in the gravitational field or drop time t_d [see Fig. 1(b)], it is also possible to infer the value of g.

A simple technique for narrowing the spectral feature to attain better precision involves increasing the duration of the excitation pulses τ. However, as shown in Ref. [42], excitation pulses cannot be extended indefinitely because motional effects due to channeling in the standing-wave potential begin to dominate.

Another method of narrowing the spectral response of the lattice contrast relies on the application of Ramsey's method of time-separated oscillatory fields (TSOFs) [44,45]. This technique has inspired efforts to improve the precision of atomic clocks that manipulate atoms between two hyperfine ground states using laser and microwave excitation [46,47].

The Ramsey technique is also the basis for Raman interferometry [1,48]. This class of experiments, widely used for inertial sensing and measurements of atomic recoil, involves manipulating atoms between multiple hyperfine ground states [2,49] but has also been adapted for interferometry involving a single ground state [50,51].

Here, we realize an improved TSOF c.m. velocimeter by exposing the atomic sample to two excitation pulses, each of duration τ, separated by a time interval T. As in the case of the single-pulse velocimeter, both excitation pulses consist of detuned counterpropagating laser fields.

In this manner it is possible to imprint a Ramsey fringe onto the lattice contrast as given by

$$\mathcal{C}(\tau, \Delta_0, T) \propto \left(\frac{\sin \Delta_0 \tau}{\Delta_0 \tau}\right)^2 \times \left\{A + 2\mathcal{D}\left[\cos^2\left(\frac{\Delta_0 T_{\text{eff}}}{2} + \phi_l\right) - 1\right]\right\}, \tag{3}$$

where $T_{\text{eff}} = T + \tau$ is the time between the centers of the two excitation pulses, and A is a proportionality constant. The unitless parameter $\mathcal{D}$ describes the Ramsey fringe contrast and represents the Gaussian FID of the atomic lattice. The cosine dependence of the lattice contrast allows the fringe width to be decreased without increasing the interaction time τ. We also incorporate a phase shift ϕ_l, to account for phase differences between the two excitation pulses.

As with the single-pulse velocimeter, we infer the lattice contrast of the TSOF velocimeter by recording the backscattered intensity of a traveling-wave readout field, as shown in Fig. 1(b). Accordingly, it is possible to achieve an improvement in precision of the c.m. velocity based on a careful measurement of the narrowed line center. Similarly, a determination of g is also possible if the Ramsey fringe is imprinted at multiple drop times by delaying the onset of the velocimeter pulse sequence.

We demonstrate these ideas using a sample of laser-cooled rubidium atoms confined in a long glass tube in a magnetically isolated environment. The apparatus, which is described in Refs. [42,43,52,53], ensures efficient polarization gradient cooling [54] and results in samples containing $\sim 10^9$ ^{85}Rb atoms at a temperature of ~ 10 μK. Laser excitation is achieved using counterpropagating pulses along the vertical [see Fig. 1(a)]. The excitation beams are circularly polarized (σ^+-σ^+) and detuned ≈400 MHz above the $(5S_{1/2})F = 3 \rightarrow (5P_{3/2})F' = 4'$ resonance in ^{85}Rb. The relative detuning between these pulses is controlled using a homebuilt radio-frequency synthesizer with an accuracy of 1 Hz, stabilized by a 10-MHz rubidium atomic clock with an Allan deviation floor value of 3×10^{-13} at 1 h.

The contrast of the lattice is optically probed with a σ^+-polarized readout pulse tuned ≈20 MHz below the same atomic resonance and traveling upward along the same path

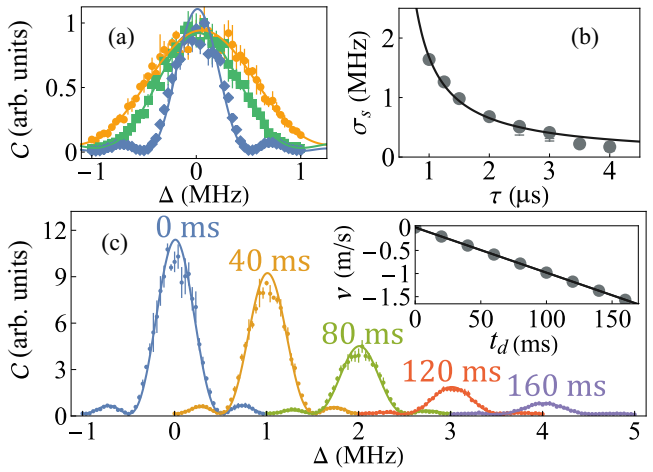

FIG. 2. (a) Lattice contrast spectra for the single-pulse velocimeter with pulse durations of 1 μs (yellow), 1.25 μs (green), and 2.5 μs (blue). The solid lines show fits to Eq. (1) for data collected across several days from samples with slightly different c.m. velocities at $t_d \approx 0$ ms. (b) Width of the contrast line shape (σ_s) as a function of pulse duration with a $1/\tau$ trend line. (c) Single-pulse velocimeter contrast spectra using $\tau = 2.5$ μs, for samples interrogated at various drop times (embedded labels). The solid lines show fits to Eq. (1). Inset: Velocity extracted from line centers using Eq. (2). Each velocity determination has an error of ≈1.4 mm/s, which is smaller than the size of the points. These data are fit to a line which gives a determination of g with an uncertainty of $\approx 4.5 \times 10^{-4} g$.

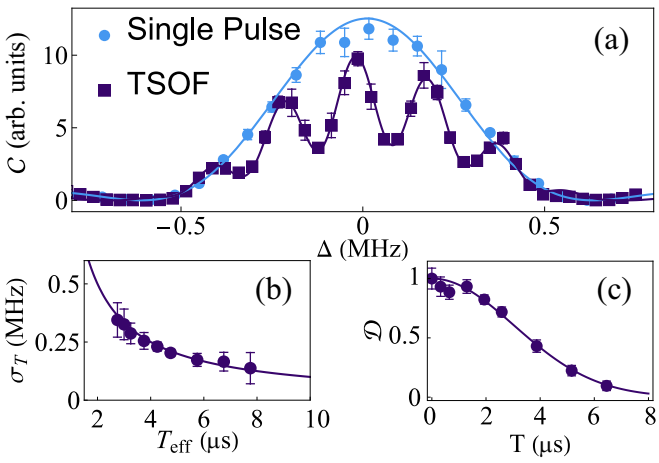

FIG. 3. (a) Contrast spectra for the single-pulse and TSOF velocimeters. $\tau = 2.5$ μs for all excitation pulses and $T = 3$ μs in the TSOF method. The solid lines are fits to Eqs. (1) and (3). (b) The period of the Ramsey fringe (σ_T) as a function of T_{eff}, showing a $1/T_{\text{eff}}$ trend line. (c) Measurements of $\mathcal{D}$ showing the decay of the Ramsey fringe contrast as a function of the time separation T. The solid line shows a Gaussian fit $\mathcal{D}(T) = e^{-(T/\tau_{\text{coh}})^2}$, where τ_{coh} gives $\mathcal{T} \sim 5$ μK.

as the excitation beam [43]. The backscattered light intensity is captured by a photomultiplier tube (PMT) that is gated immediately before the onset of the readout pulse as in Refs. [42,43]. The PMT signal, which is averaged over four repetitions, has a characteristic decay time constant $\tau_{\text{coh}} = 1/(ku)$ as shown in Fig. 1(c), where k is the wave vector of the excitation and $u = \sqrt{2k_B\mathcal{T}/M}$ is the most probable thermal speed. Here, k_B is Boltzmann's constant, M is the atomic mass, and $\mathcal{T}$ is the temperature of the sample.

Figure 2(a) shows the lattice contrast spectrum of the single-pulse velocimeter as a function of Δ, the relative frequency difference between the two components of the excitation pulse in the laboratory frame. We find that these data are well modeled by Eq. (1) and that the width of the spectral feature scales inversely with τ, as shown by Fig. 2(b). Here, we limit the pulse duration to avoid any channeling effects [42].

Figure 2(c) shows multiple contrast spectra recorded at different drop times, where the first-order Doppler shift is manifested as a shift in the position of the line center. We find that the c.m. velocity can be extracted from the center of each spectrum using Eq. (2) with a precision of ≈1.4 mm/s. The inset to Fig. 2(c) shows the determination of g that can be made by fitting to the linear dependence of the velocity as a function of drop time. Using this technique, we find that g can be measured to ≈500 parts per million (ppm) with the single-pulse velocimeter. The precision of these v and g determinations is primarily limited by the width of the spectral feature.

Figure 3(a) shows a comparison of contrast spectra for the single-pulse and TSOF velocimeters. Both spectra were obtained using identical pulse durations of $\tau = 2.5$ μs. The data are well modeled by Eqs. (1) and (3), and the decrease in the width of the TSOF spectrum is readily evident. The value of ϕ_l for these curves is 0.18π which arises from a phase-shifting delay line in the radio-frequency network for the second excitation pulse.

We investigate the behavior of the Ramsey fringe pattern by increasing the pulse separation T. As expected, the fringe width exhibits a $1/T_{\text{eff}}$ dependence as shown in Fig. 3(b). The limitation on the TSOF velocimeter is determined by the coherence time of the sample. To observe this limitation, we plot the Ramsey fringe contrast ($\mathcal{D}$) as a function of the time separation between pulses in Fig. 3(c). Since $\mathcal{D}$ is determined by the FID of the lattice, it is expected that the contrast of the Ramsey fringe will decrease as the pulse separation is increased. From the Gaussian fit, we find the coherence time to be ≈4 μs which implies a sample temperature of ∼5 μK, consistent with independent time-of-flight measurements using a CCD camera [52,55].

Figure 3 also highlights a desirable feature of the technique, that it is not necessary to convolve the atomic response in Eqs. (1) and (3) with the velocity distribution of the sample if $T < \tau_{\text{coh}}$. Since the Ramsey signal can only be realized within the coherence time of the sample, this condition is guaranteed in the TSOF configuration. Accordingly, a narrow TSOF line shape could also be used for probing other spectral shifts, such as those arising from electric and magnetic fields, in addition to gravitational fields.

Figure 4 shows TSOF velocimeter contrast spectra recorded at different drop times with accompanying fits to Eq. (3). As expected, the value of ϕ_l remains constant for these spectra, since it arises from the relative phase difference of the excitation beams and not the c.m. velocity of the sample. In comparison with the single-pulse velocimeter, we find an improved sensitivity to c.m. velocity of ≈600 μm/s due to

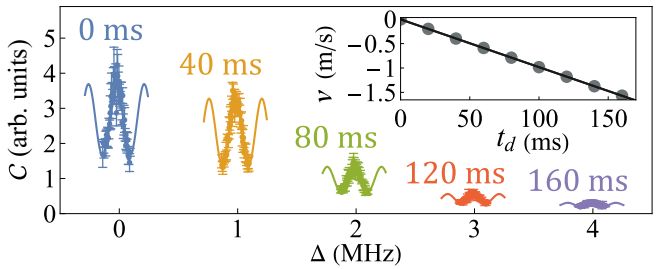

FIG. 4. Contrast spectra for the TSOF velocimeter with $\tau = 2.5$ μs and $T = 3$ μs. Signals correspond to a single Ramsey fringe collected for samples interrogated at various drop times (embedded labels). Solid lines represent fits to Eq. (3). Inset: The extracted velocities as a function of drop time. Each determination has a precision of ≈600 μm/s leading to a measurement of g (linear trend line) with a precision of $\approx 2 \times 10^{-4} g$.

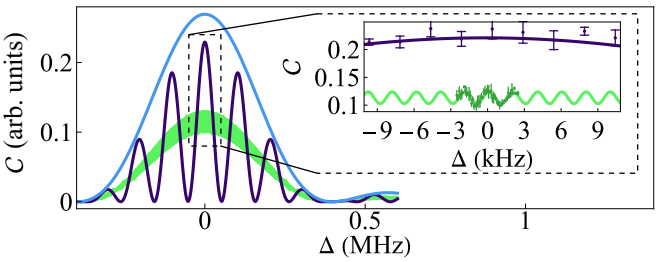

FIG. 5. Simulation of contrast spectra for a single-pulse velocimeter (light blue, $\tau = 2.5$ μs), a short-timescale TSOF velocimeter (dark blue, $\tau = 2.5$ μs and $T = 2.5$ μs), and a TSOF velocimeter with a large pulse separation (green, $\tau = 2.5$ μs and $T = 250$ μs), using a sample with $\mathcal{T} \approx 1$ nK. Inset: Zoomed in image where simulated data are fit to Eq. (3) (solid lines), giving a velocity uncertainty of ≈5 μm/s for the long-timescale TSOF velocimeter.

the narrowed TSOF spectra. Similarly, the inset shows an improved measurement of g with a precision of ≈200 ppm using the TSOF velocimeter. As in the case of the single-pulse velocimeter, the value of g is determined from a linear fit to nine velocity measurements obtained with drop times ranging up to 160 ms.

Although the precision of the TSOF velocimeter (600 μm/s) is about an order of magnitude less sensitive than that of the best cold-atom-based velocimeter [32] (≈70 μm/s), these experiments highlight a particularly attractive feature, namely that the phase of the laser excitation only needs to be maintained over the time interval T. In other cold-atom sensors, such as atom interferometers [15,32], phase stability is required over the entire drop interval, imposing the need for phase monitoring and correction since pulse separations on the order of many milliseconds are strongly affected by mechanical vibrations.

A compelling aspect of this work is the potential for achieving vastly improved results by employing the TSOF velocimeter in a different class of atomic samples, namely Bose-Einstein condensates (BECs) and Fermi gases. Since the primary limitation of the TSOF velocimeter arises from the narrowest fringe width that can be attained within the coherence time of the sample, the precision can be substantially improved by operating with BECs and Fermi gases, which are now widely used. For example, Refs. [56,57] use coherent backscattering from BEC to observe matter-wave fringes, while Ref. [58] spatially resolves Ramsey fringes imprinted using Bragg pulses in a Fermi gas.

To estimate the ultimate sensitivity of the TSOF velocimeter, we consider a Bose gas with a coherence time of ∼300 μs and simulate the contrast spectra shown in Fig. 5, incorporating a similar level of noise as in the experiments presented in this Letter. Using a moderate pulse separation of $T = 250$ μs, which is readily achievable in BEC experiments, we project a c.m. velocity determination with a precision of ≈5 μm/s, and observe that the contrast remains well above the noise floor of our experiment. These results surpass the performance of cold-atom velocimeters by almost an order of magnitude and rival the most precise atomic velocimeter [30].

Despite the linear T-dependent improvement in precision of velocimetric measurements, compared to the T^2 scaling of conventional accelerometers, the simulations also suggest that g can be determined with a precision of 1 ppm using a tabletop TSOF velocimeter, with $T = 250$ μs and a 200 ms drop time. However, since BEC interferometers have reported maintaining spatial coherence over timescales of several milliseconds [56,57] and drop towers are designed for ∼1 s drop times [17,18,23], it becomes realistic to consider extending both of these timescales.

In such experiments, with large values of T where g causes the sample velocity to change in between excitation pulses, the central fringe can be identified by chirping the frequency difference of the excitation components during the pulse separation to maintain the two-photon resonance. The TSOF pattern, shown by the green curve in the inset to Fig. 5, can be recovered as a function of the chirp rate for each value of T. In this manner, measurements at a variety of T separations can be combined to remove the ambiguity in the central fringe, a technique widely used in Raman interferometry [15]. In addition, the measurement protocol will need to be modified since the backscattered signal will be modulated by atomic recoil on timescales of T larger than the recoil period [36,56,57].

Under these conditions, the combination of a ∼1 s drop time and a pulse separation of ∼10 ms in the TSOF velocimeter should allow for measurements of v precise at the level of 1 μm/s and determinations of g with an uncertainty of less than 10 parts per billion (ppb). Here again, despite the long drop time, since the TSOF velocimeter relies on the matter-wave interference effect responsible for FID, it will only require phase stability over the pulse separation of ∼10 ms rather than the extraordinarily long drop time of order 1 s possible in a large tower.

This work is supported by Canada Foundation for Innovation, Ontario Innovation Trust, Ontario Centers of Excellence, U.S. Army Research Office (Grant No. W911 NF-12-1-0564), Natural Sciences and Engineering Research Council of Canada, York University, and the Helen Freedhoff Memorial Fund. We also acknowledge helpful discussions with Louis Marmet of York University.

[1] M. Kasevich and S. Chu, Atomic interferometry using stimulated Raman transitions, Phys. Rev. Lett. **67**, 181 (1991).

[2] A. Peters, K. Y. Chung, and S. Chu, Measurement of gravitational acceleration by dropping atoms, Nature (London) **400**, 849 (1999).

[3] Z.-K. Hu, B.-L. Sun, X.-C. Duan, M.-K. Zhou, L.-L. Chen, S. Zhan, Q.-Z. Zhang, and J. Luo, Demonstration of an ultrahigh-sensitivity atom-interferometry absolute gravimeter, Phys. Rev. A **88**, 043610 (2013).

[4] J. M. McGuirk, G. T. Foster, J. B. Fixler, M. J. Snadden, and M. A. Kasevich, Sensitive absolute-gravity gradiometry using atom interferometry, Phys. Rev. A **65**, 033608 (2002).

[5] M. J. Snadden, J. M. McGuirk, P. Bouyer, K. G. Haritos, and M. A. Kasevich, Measurement of the Earth's gravity gradient with an atom interferometer-based gravity gradiometer, Phys. Rev. Lett. **81**, 971 (1998).

[6] A. V. Rakholia, H. J. McGuinness, and G. W. Biedermann, Dual-axis high-data-rate atom interferometer via cold ensemble exchange, Phys. Rev. Appl. **2**, 054012 (2014).

[7] T. Gustavson, A. Landragin, and M. Kasevich, Rotation sensing with a dual atom-interferometer Sagnac gyroscope, Class. Quantum Grav. **17**, 2385 (2000).

[8] T. L. Gustavson, P. Bouyer, and M. A. Kasevich, Precision rotation measurements with an atom interferometer gyroscope, Phys. Rev. Lett. **78**, 2046 (1997).

[9] B. Canuel, F. Leduc, D. Holleville, A. Gauguet, J. Fils, A. Virdis, A. Clairon, N. Dimarcq, C. J. Bordé, A. Landragin, and P. Bouyer, Six-axis inertial sensor using cold-atom interferometry, Phys. Rev. Lett. **97**, 010402 (2006).

[10] B. Barrett, L. Antoni-Micollier, L. Chichet, B. Battelier, T. Léveque, A. Landragin, and P. Bouyer, Dual matter-wave inertial sensors in weightlessness, Nat. Commun. **7**, 13786 (2016).

[11] B. Battelier, B. Barrett, L. Fouché, L. Chichet, L. Antoni-Micollier, H. Porte, F. Napolitano, J. Lautier, A. Landragin, and P. Bouyer, Development of compact cold-atom sensors for inertial navigation, Proc. SPIE **9900**, 990004 (2016).

[12] Y. Bidel, N. Zahzam, C. Blanchard, A. Bonnin, M. Cadoret, A. Bresson, D. Rouxel, and M. Lequentrec-Lalancette, Absolute marine gravimetry with matter-wave interferometry, Nat. Commun. **9**, 627 (2018).

[13] Y. Bidel, N. Zahzam, A. Bresson, C. Blanchard, M. Cadoret, A. V. Olesen, and R. Forsberg, Absolute airborne gravimetry with a cold atom sensor, J. Geodesy **94**, 20 (2020).

[14] B. Stray, A. Lamb, A. Kaushik, J. Vovrosh, A. Rodgers, J. Winch, F. Hayati, D. Boddice, A. Stabrawa, A. Niggebaum *et al.*, Quantum sensing for gravity cartography, Nature (London) **602**, 590 (2022).

[15] X. Wu, Z. Pagel, B. S. Malek, T. H. Nguyen, F. Zi, D. S. Scheirer, and H. Müller, Gravity surveys using a mobile atom interferometer, Sci. Adv. **5**, eaax0800 (2019).

[16] C. Freier, M. Hauth, V. Schkolnik, B. Leykauf, M. Schilling, H. Wziontek, H.-G. Scherneck, J. Müller, and A. Peters, Mobile quantum gravity sensor with unprecedented stability, J. Phys.: Conf. Ser. **723**, 012050 (2016).

[17] T. Könemann, W. Brinkmann, E. Göklü, C. Lämmerzahl, H. Dittus, T. Van Zoest, E. Rasel, W. Ertmer, W. Lewoczko-Adamczyk, M. Schiemangk *et al.*, A freely falling magneto-optical trap drop tower experiment, Appl. Phys. B **89**, 431 (2007).

[18] C. Deppner, W. Herr, M. Cornelius, P. Stromberger, T. Sternke, C. Grzeschik, A. Grote, J. Rudolph, S. Herrmann, M. Krutzik, A. Wenzlawski, R. Corgier, E. Charron, D. Guéry-Odelin, N. Gaaloul, C. Lämmerzahl, A. Peters, P. Windpassinger, and E. M. Rasel, Collective-mode enhanced matter-wave optics, Phys. Rev. Lett. **127**, 100401 (2021).

[19] H. Müntinga, H. Ahlers, M. Krutzik, A. Wenzlawski, S. Arnold, D. Becker, K. Bongs, H. Dittus, H. Duncker, N. Gaaloul, C. Gherasim, E. Giese, C. Grzeschik, T. W. Hänsch, O. Hellmig, W. Herr, S. Herrmann, E. Kajari, S. Kleinert, C. Lämmerzahl *et al.*, Interferometry with Bose-Einstein condensates in microgravity, Phys. Rev. Lett. **110**, 093602 (2013).

[20] S. Herrmann, H. Dittus, C. Lämmerzahl *et al.*, Testing the equivalence principle with atomic interferometry, Class. Quantum Grav. **29**, 184003 (2012).

[21] G. Lamporesi, A. Bertoldi, L. Cacciapuoti, M. Prevedelli, and G. M. Tino, Determination of the newtonian gravitational constant using atom interferometry, Phys. Rev. Lett. **100**, 050801 (2008).

[22] M. G. Tarallo, T. Mazzoni, N. Poli, D. V. Sutyrin, X. Zhang, and G. M. Tino, Test of Einstein equivalence principle for 0-spin and half-integer-spin atoms: Search for spin-gravity coupling effects, Phys. Rev. Lett. **113**, 023005 (2014).

[23] C. Overstreet, P. Asenbaum, T. Kovachy, R. Notermans, J. M. Hogan, and M. A. Kasevich, Effective inertial frame in an atom interferometric test of the equivalence principle, Phys. Rev. Lett. **120**, 183604 (2018).

[24] P. Asenbaum, C. Overstreet, T. Kovachy, D. D. Brown, J. M. Hogan, and M. A. Kasevich, Phase shift in an atom interferometer due to spacetime curvature across its wave function, Phys. Rev. Lett. **118**, 183602 (2017).

[25] P. Asenbaum, C. Overstreet, M. Kim, J. Curti, and M. A. Kasevich, Atom-interferometric test of the equivalence principle at the 10^{-12} level, Phys. Rev. Lett. **125**, 191101 (2020).

[26] W. Gong, A. Li, C. Huang, H. Che, C. Feng, and F. Qin, Effects and prospects of the vibration isolation methods for an atomic interference gravimeter, Sensors **22**, 583 (2022).

[27] G. D'Amico, L. Cacciapuoti, M. Jain, S. Zhan, and G. Rosi, Measuring the gravitational acceleration with matter-wave velocimetry, Eur. Phys. J. D **73**, 98 (2019).

[28] R. Shaniv and R. Ozeri, Quantum lock-in force sensing using optical clock Doppler velocimetry, Nat. Commun. **8**, 14157 (2017).

[29] P.-C. Kuan, C. Huang, W. S. Chan, S. Kosen, and S.-Y. Lan, Large Fizeau's light-dragging effect in a moving electromagnetically induced transparent medium, Nat. Commun. **7**, 13030 (2016).

[30] Z. Chen, H. M. Lim, C. Huang, R. Dumke, and S.-Y. Lan, Quantum-enhanced velocimetry with Doppler-broadened atomic vapor, Phys. Rev. Lett. **124**, 093202 (2020).

[31] M. Kasevich, D. S. Weiss, E. Riis, K. Moler, S. Kasapi, and S. Chu, Atomic velocity selection using stimulated Raman transitions, Phys. Rev. Lett. **66**, 2297 (1991).

[32] J. Chabé, H. Lignier, P. Szriftgiser, and J. C. Garreau, Improving Raman velocimetry of laser-cooled cesium atoms by spin-polarization, Opt. Commun. **274**, 254 (2007).

[33] G. W. Biedermann, H. J. McGuinness, A. V. Rakholia, Y.-Y. Jau, D. R. Wheeler, J. D. Sterk, and G. R. Burns, Atom interferometry in a warm vapor, Phys. Rev. Lett. **118**, 163601 (2017).

[34] E. J. Su, S. Wu, and M. G. Prentiss, Atom interferometry using wave packets with constant spatial displacements, Phys. Rev. A **81**, 043631 (2010).

[35] C. Mok, B. Barrett, A. Carew, R. Berthiaume, S. Beattie, and A. Kumarakrishnan, Demonstration of improved sensitivity of echo interferometers to gravitational acceleration, Phys. Rev. A **88**, 023614 (2013).

[36] S. B. Cahn, A. Kumarakrishnan, U. Shim, T. Sleator, P. R. Berman, and B. Dubetsky, Time-domain de Broglie wave interferometry, Phys. Rev. Lett. **79**, 784 (1997).

[37] B. Barrett, I. Chan, C. Mok, A. Carew, I. Yavin, A. Kumarakrishnan, S. B. Cahn, and T. Sleator, Time-domain interferometry with laser-cooled atoms, in *Advances in Atomic, Molecular, and Optical Physics*, Vol. 60 (Elsevier, Amsterdam, 2011), pp. 119–199.

[38] M. Weel, I. Chan, S. Beattie, A. Kumarakrishnan, D. Gosset, and I. Yavin, Effect of a magnetic field gradient and gravitational acceleration on a time-domain grating-echo interferometer, Phys. Rev. A **73**, 063624 (2006).

[39] S. Beattie, B. Barrett, M. Weel, I. Chan, C. Mok, S. B. Cahn, and A. Kumarakrishnan, Influence of spontaneous emission on a single-state atom interferometer, Phys. Rev. A **77**, 013610 (2008).

[40] B. Barrett, I. Chan, and A. Kumarakrishnan, Atom-interferometric techniques for measuring uniform magnetic field gradients and gravitational acceleration, Phys. Rev. A **84**, 063623 (2011).

[41] B. Barrett, A. Carew, S. Beattie, and A. Kumarakrishnan, Measuring the atomic recoil frequency using a modified grating-echo atom interferometer, Phys. Rev. A **87**, 033626 (2013).

[42] G. Carlse, J. Randhawa, E. Ramos, T. Vacheresse, A. Pouliot, A. C. Carew, and A. Kumarakrishnan, Role of optical channeling in contrast enhancement of echo interferometers, Phys. Rev. A **109**, 043307 (2024).

[43] G. Carlse, J. Randhawa, E. Ramos, T. Vacheresse, A. Pouliot, A. C. Carew, A. Kumarakrishnan, and B. Barrett, Optimization of Bragg scattering from atomic gratings for echo interferometry, Phys. Rev. A **110**, 043306 (2024).

[44] N. F. Ramsey, A molecular beam resonance method with separated oscillating fields, Phys. Rev. **78**, 695 (1950).

[45] N. F. Ramsey, Experiments with separated oscillatory fields and hydrogen masers, Rev. Mod. Phys. **62**, 541 (1990).

[46] P. R. Hemmer, G. P. Ontai, and S. Ezekiel, Precision studies of stimulated-resonance Raman interactions in an atomic beam, J. Opt. Soc. Am. B **3**, 219 (1986).

[47] K. Gibble and S. Chu, Laser-cooled Cs frequency standard and a measurement of the frequency shift due to ultracold collisions, Phys. Rev. Lett. **70**, 1771 (1993).

[48] D. S. Weiss, B. C. Young, and S. Chu, Precision measurement of the photon recoil of an atom using atomic interferometry, Phys. Rev. Lett. **70**, 2706 (1993).

[49] C. Yu, W. Zhong, B. Estey, J. Kwan, R. H. Parker, and H. Müller, Atom-interferometry measurement of the fine structure constant, Ann. Phys. **531**, 1800346 (2019).

[50] B. Dubetsky and P. R. Berman, Ground-state Ramsey fringes, Phys. Rev. A **56**, R1091 (1997).

[51] M. Weel and A. Kumarakrishnan, Observation of ground-state Ramsey fringes, Phys. Rev. A **67**, 061602(R) (2003).

[52] G. Carlse, A. Pouliot, T. Vacheresse, A. Carew, H. C. Beica, S. Winter, and A. Kumarakrishnan, Technique for magnetic moment reconstruction of laser-cooled atoms using direct imaging and prospects for measuring magnetic sublevel distributions, J. Opt. Soc. Am. B **37**, 1419 (2020).

[53] B. Barrett, A. Carew, H. C. Beica, A. Vorozcovs, A. Pouliot, and A. Kumarakrishnan, Prospects for precise measurements with echo atom interferometry, Atoms **4**, 19 (2016).

[54] C. G. Townsend, N. H. Edwards, C. J. Cooper, K. P. Zetie, C. J. Foot, A. M. Steane, P. Szriftgiser, H. Perrin, and J. Dalibard, Phase-space density in the magneto-optical trap, Phys. Rev. A **52**, 1423 (1995).

[55] A. Vorozcovs, M. Weel, S. Beattie, S. Cauchi, and A. Kumarakrishnan, Measurements of temperature scaling laws in an optically dense magneto-optical trap, J. Opt. Soc. Am. B **22**, 943 (2005).

[56] S. Gupta, K. Dieckmann, Z. Hadzibabic, and D. E. Pritchard, Contrast interferometry using Bose-Einstein condensates to measure h/m and α, Phys. Rev. Lett. **89**, 140401 (2002).

[57] A. O. Jamison, B. Plotkin-Swing, and S. Gupta, Advances in precision contrast interferometry with Yb Bose-Einstein condensates, Phys. Rev. A **90**, 063606 (2014).

[58] B. Deh, C. Marzok, S. Slama, C. Zimmermann, and P. W. Courteille, Bragg spectroscopy and Ramsey interferometry with an ultracold Fermi gas, Appl. Phys. B **97**, 387 (2009).